International Symposium
On Turbulence and Shear Flow
Phenomena (TSFP-8)
August 28 - 30, 2013 Poitiers, France

MEASUREMENTS OF TURBULENT DIFFUSION FROM A POINT SOURCE IN UNIFORMLY SHEARED FLOW

Christina Vanderwel
Department of Mechanical Engineering
University of Ottawa
Ottawa, Canada
christina.vanderwel@uottawa.ca

Stavros Tavoularis
Department of Mechanical Engineering
University of Ottawa
Ottawa, Canada
stavros.tavoularis@uottawa.ca

ABSTRACT

Turbulent diffusion of a plume of fluorescent dye with a very high Schmidt number and released from a point source in uniformly sheared flow was investigated in a water tunnel using stereoscopic particle image velocimetry and planar laser-induced fluorescence. Cross-sectional maps of the mean concentration and all three components of the turbulent mass flux vector are presented. A first-order gradient transport model relating each component of the turbulent mass flux vector to all components of the mean concentration gradient was applied successfully and all components of the associated turbulent diffusivity tensor were determined. The measured apparent diffusivities were comparable to the corresponding diffusivities. Predictions of three theoretical models were found to be in partial qualitative agreement with the measured diffusivities.

INTRODUCTION

Air and water pollution is the subject of intense research because of its obvious links to illness and high health cost. An important concern of environmental pollution research is the turbulent transport of pollutants from concentrated emission sources and the extent of their impact. Examples of contaminants released and dispersed in the atmosphere include, among others, particulates, carbon dioxide and various hazardous gases, emanating from natural sources, such as wildfires or volcanic eruptions, as well as from anthropogenic sources, such as power generation plants and other industrial facilities. Examples of pollutants released in the waterways include sewer material and chemical spills. In addition to the dispersal of pollutants in the environment, turbulent transport and mixing of scalar quantities are central mechanisms affecting chemical reactions, including combustion processes. Engineering predictions of turbulent diffusion are still relatively crude and mostly concerned with the mean scalar concentration field (Roberts & Webster, 2002).

The turbulent diffusion of a passive scalar with concentration C is governed by the Reynolds-averaged advection-diffusion equation

$$\underbrace{\frac{\partial \overline{C}}{\partial t} + \overline{U_i}\frac{\partial \overline{C}}{\partial x_i}}_{\text{advection}} = \underbrace{\gamma \frac{\partial^2 \overline{C}}{\partial x_i \partial x_i}}_{\text{molecular diffusion}} + \underbrace{\frac{\partial(-\overline{cu_i})}{\partial x_i}}_{\text{turbulent diffusion}}, \quad (1)$$

where $\overline{C}$ is the mean concentration, $\overline{U_i}$ is the mean velocity vector, γ is the molecular diffusivity, and $\overline{cu_i}$ is the concentration-velocity covariance or turbulent mass flux vector. To solve this equation for $\overline{C}$, one needs a closure model for the turbulent mass flux vector. The most commonly used model is the first-order gradient transport model (Arya, 1999)

$$-\overline{cu_i} = D_{ij}\frac{\mathrm{d}\overline{C}}{\mathrm{d}x_j}, \quad (2)$$

where D_{ij} is the turbulent (or "eddy") diffusivity tensor. The limitations of the gradient transport model are well known (Corrsin, 1974). The most significant limitation is that a gradient transport assumption is only valid when the characteristic lengthscale of the scalar is much greater than that of the transporting mechanism (*i.e.*, the turbulence). Sreenivasan *et al.* (1982) pointed out that although this requirement is violated in most turbulent flows, the gradient transport model is still rather successful and widely used.

A theoretical analysis of the turbulent diffusion tensor was first presented by Batchelor (1949), who defined the diffusion coefficient tensor K_{ij} in terms of the mean Lagrangian displacement tensor $\overline{\mathbf{X}_i\mathbf{X}_j}(t)$ of a particle transported by homogeneous turbulence as

$$K_{ij}(t) = \frac{1}{2}\frac{\mathrm{d}\overline{\mathbf{X}_i\mathbf{X}_j}}{\mathrm{d}t}. \quad (3)$$

He further demonstrated that, for a single-particle dispersion in homogeneous turbulence without shear, and assuming a Gaussian particle displacement distribution, K_{ij} would be equivalent to D_{ij}, as defined in eq. 2. Batchelor also showed that, in isotropic turbulence, D_{ij} would be proportional to the identity tensor (Kronecker's delta); its magnitude would be initially zero at the moment the particle is released, it would increase with dispersion time, and it would eventually reach an asymptote.

For a cloud of particles released instantaneously at a point in a turbulent flow with no mean velocity, $\overline{\mathbf{X}_i^2}(t)$ is a measure of the spread of the cloud along the axis x_i. The plume generated by a continuously emitting source may be considered as the result of superposition of clouds emitted successively be an instantaneous source. For a plume of particles emitted from a point source in a turbulent flow with a uniform mean velocity U_1, the apparent diffusivities in the two normal directions are defined as

$$K_2 = \frac{U_1}{2}\frac{\mathrm{d}\sigma_2^2}{\mathrm{d}x_1}, \quad K_3 = \frac{U_1}{2}\frac{\mathrm{d}\sigma_3^2}{\mathrm{d}x_1}, \tag{4}$$

where σ_2 and σ_3 are the corresponding characteristic plume widths. Only if the streamwise dispersion is negligible will the apparent plume diffusivities K_2 and K_3 be equivalent to the diffusion coefficients K_{22} and K_{33} (Arya, 1999), and thus to D_{22} and D_{33}.

Riley & Corrsin (1974) expanded Batchelor's analysis for homogeneous turbulent shear flow and noted that the normal diffusivities were unequal and that one cross-diffusivity was not zero. Asymptotic expressions for the turbulent diffusivity tensor components in shear flows have been derived from theoretical arguments by Tavoularis & Corrsin (1985), Rogers *et al.* (1989) and Younis *et al.* (2005).

The objective of this work is to study experimentally turbulent dispersion in the laboratory and specifically to measure all components of the turbulent diffusivity tensor. The statistical properties of the velocity and scalar concentration fields in a plume released passively from a point source in nearly homogeneous turbulent shear flow were measured simultaneously on cross-sectional planes using stereoscopic particle image velocimetry (SPIV) and planar laser-induced fluorescence (PLIF). Thus, two-dimensional maps of the three concentration-velocity covariances were obtained, in contrast to previous studies, which reported only point measurements in a plume from a point source (Nakamura *et al.*, 1986) and a plume from a line source (Karnik & Tavoularis, 1989). From these maps and maps of the mean scalar concentration, the values of all components of the turbulent diffusivity tensor were determined directly via eq. 2. This is the first time all nine components of the turbulent diffusivity tensor have been determined together experimentally. These experimental results will also be compared to theoretical estimates of the diffusivity ratios.

APPARATUS AND FLOW CONDITIONS

The experiments have been conducted in a recirculating, free-surface water tunnel (fig. 1), having a test section with a width of 0.53 m, a length of about 4 m, and filled to a depth of 0.46 m. Uniformly sheared flow (USF) was generated by a perforated plate of varying solidity ("shear generator"), inserted at the entrance to the test section and followed by an array of plates spaced by a distance of L = 25.4 mm ("flow separator").

A neutrally buoyant aqueous solution of Rhodamine 6G fluorescent dye with an initial concentration C_S = 0.3 mg/ℓ was injected into the flow through a fine tube having a tip with an inner diameter of 1.83 mm and a wall thickness of 0.15 mm. To minimize its disturbance to the flow, the tube was inserted in the stream through the flow separator and was aligned with the flow section centreline so that the dye was discharged at approximately 2 m downstream of the flow separator, where the turbulence structure of the USF was fully developed. The injection tube was tethered by 50 μm thick guide wires, and was free of any movement or vibrations. The dye solution flow rate was adjusted so that its injection created the least possible flow disturbance. The dye is known to have a molecular diffusivity of $\gamma = (4.0 \pm 0.3) \times 10^{-4}$ mm^2/s (Gendron *et al.*, 2008), which corresponds to a Schmidt number of $Sc \equiv \nu/\gamma = 2500 \pm 300$.

Velocity and concentration measurements were taken simultaneously in cross sections of the flow that were illuminated by a light sheet created from the output of a Nd:YAG pulsed laser. Velocity measurements were performed using a two-camera SPIV system (LaVision FlowMaster). Concentration measurements were performed using a third camera (PCO-Edge), synchronized with the SPIV system and the laser pulses. In a manner similar to the LIF analysis of Webster *et al.* (2003), the concentration C of the dye measured by each pixel of the camera was determined from the intensity F of the dye fluorescence in the plane of the laser sheet by the following equation

$$\frac{C(x_2,x_3)}{C_{\mathrm{cal}}} = \frac{F(x_2,x_3) - F_o(x_2,x_3)}{F_{\mathrm{cal}}(x_2,x_3) - F_o(x_2,x_3)}. \tag{5}$$

In this equation, F_{cal} is the calibration measurement corresponding to a uniform concentration of C_{cal} = 0.075 mg/ℓ and F_o is the camera reading when there was no dye in the field of view. This method was tested by taking measurements in several dye mixtures with uniform and known concentrations; the overall concentration measurement uncertainty was estimated to be about 5% of the local measured value of C. The spatial resolutions of the measured velocity and concentration fields were, respectively, one vector per 1.15 mm × 1.15 mm flow area and one scalar sample per 0.05 mm × 0.05 mm area.

The USF and its turbulence structure have been documented previously by Vanderwel & Tavoularis (2011). In the present tests, the undisturbed mean velocity at the point of dye injection was U_C = 0.18 m/s, the mean shear was $d\overline{U}_1/dx_2 = 0.6$ s^{-1}, the shear rate parameter was $S^* \equiv (2k/\varepsilon)(d\overline{U}_1/dx_2) \approx 17$, and the turbulent Reynolds number was $Re_\lambda \approx 160$. The Kolmogorov and Batchelor microscales were 0.60 mm and 0.012 mm, respectively. The turbulent stresses were essentially homogeneous on planes normal to the flow direction but grew in the streamwise direction (*e.g.*, u_2'/U_C grew from 3.4 to 4% in the range of the plume). The turbulent viscosity $\nu_T \equiv -\overline{u_1 u_2}/(d\overline{U}_1/dx_2)$ grew from 34 to 58 mm^2/s in the range of the plume. The integral length-scales grew slightly along the plume, albeit maintaining values not far from the flow separator spacing L.

RESULTS

Mean concentration maps

A representative mean concentration map $\overline{C}/C_S$ is provided in fig. 2. For $x_1/L \geq 5$, the mean concentration

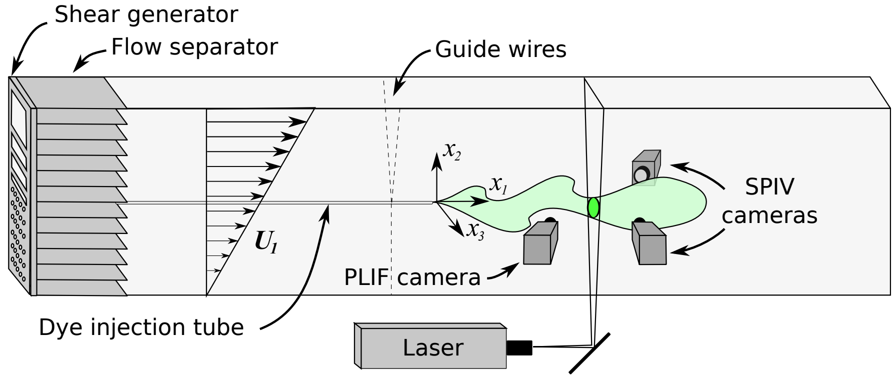

Figure 1: Sketch of the experimental apparatus and main instrumentation in the water tunnel test section.

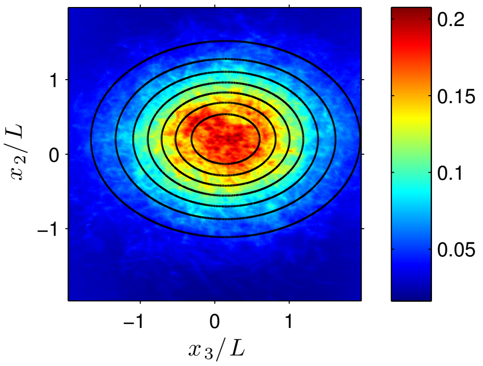

Figure 2: Map of the normalized mean concentration of the plume $\frac{\overline{C}}{C_S}/\frac{A}{\sigma_2\sigma_3}$ at $x_1/L = 28$. Black ellipses are isocontours of the fitted 2D Gaussian function.

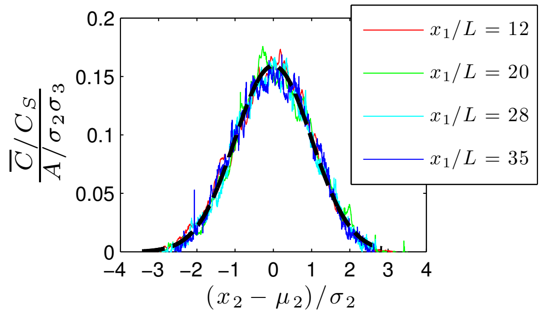

Figure 3: Vertical profiles of the mean concentration at several streamwise locations, normalized by the local Gaussian fit parameters; a Gaussian function, plotted as a dashed line, fits well to all measurements.

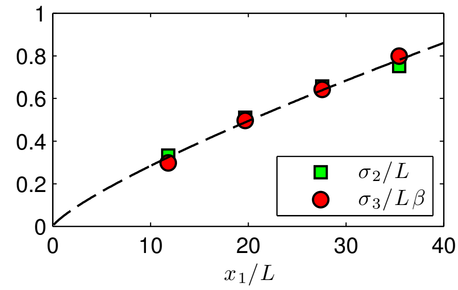

Figure 4: Streamwise evolutions of the dimensionless transverse plume width σ_2/L and the scaled spanwise plume width $\sigma_3/(L\beta)$ ($\beta = 1.4$). The dashed line indicates the fitted power law, $0.045(x_1/L)^{0.8}$.

map could be fitted fairly well by the 2D Gaussian function (fig. 3)

$$\frac{\overline{C}}{C_S} = \frac{A}{2\pi\sigma_2\sigma_3}\exp\left[-\frac{(x_2-\mu_2)^2}{2\sigma_2^2} - \frac{(x_3-\mu_3)^2}{2\sigma_3^2}\right], \qquad (6)$$

where μ_2 and μ_3 are the transverse and spanwise coordinates of the mean plume axis and σ_2^2 and σ_3^2 are the corresponding second central moments of the concentration distribution. The mean plume axis did not deviate significantly from the streamwise direction ($|\mu_2|, |\mu_3| < 0.3L$); this differs from the observations by Karnik & Tavoularis (1989) and Nakamura *et al.* (1986) that their plume axes drifted towards the lower velocity region of their USF.

The transverse σ_2 and spanwise σ_3 plume widths grew consistently in the streamwise direction (fig. 4). Both trends were described well by power laws having the same exponent of $n = 0.8$, which is close to the value of $n = 0.83$ by Karnik & Tavoularis and within the range of $0.45 < n < 0.95$ by Nakamura *et al.*. Their ratio was $\sigma_3/\sigma_2 = 1.4 \pm 0.1$, which reflects the fact that $u_3' > u_2'$. Substitution of the power laws into eq. 4 provided the transverse apparent diffusivity as $K_2/(U_C L) = 0.0016\,(x_1/L)^{0.6}$ and the apparent diffusivity ratio as $K_3/K_2 = 2.0 \pm 0.3$.

Estimates of turbulent diffusivities

In the present experiments, cross-sectional maps of all components of the turbulent mass flux vector $\overline{cu_i}$ were obtained following resampling and interpolation of the SPIV measurements to the same grid as the PLIF ones. Cross-sectional maps of all components of the mean concentration gradient $\mathrm{d}\overline{C}/\mathrm{d}x_i$ were also independently determined by analytical differentiation of eq. 6. This permitted the calculation of all nine components of the turbulent diffusivity tensor D_{ij} as those values that resulted in the best fit between the left- and right-hand sides of eq. 2 over each set of corresponding map pairs. The cross components D_{13}, D_{23}, D_{31} and D_{32} should vanish because of the symmetry of the Reynolds stress tensor and the scalar field about the $(x_1 - x_3)$ plane; therefore, these diffusivities were set to zero before calculating the other components (preliminary calculations, to be discussed shortly, confirmed that the effects of these components were indeed negligible in the present flow). Representative maps of the scalar fluxes at $x_1/L = 28$ are presented in fig. 5. The same figure also shows cross-sections of these maps, together with profiles of the relevant terms of the right-hand side of eq. 2. The streamwise evolution of the estimated D_{22} is plotted in fig. 6a, whereas figs. 6b-e show the evolutions of the ratios of the remaining non-zero diffusivities and D_{22}. It may be seen that there is considerable uncertainty in these results, much of which is attributed to the uncertainty of the streamwise scalar gradient. Simplified estimates of D_{22} and D_{33} were obtained as the slopes of linear fits to the scatter plots of $\overline{cu_2}$ vs. $\mathrm{d}\overline{C}/\mathrm{d}x_2$ and $\overline{cu_3}$ vs. $\mathrm{d}\overline{C}/\mathrm{d}x_3$; these estimates differed from those presented previously by 4% and 1%, respectively, which attests to the fact that the neglected terms in the calculation of the corresponding diffusivities were indeed negligible.

A secondary approach for estimating the turbulent diffusivities is by assuming that gradient transport also applies to third-order concentration-velocity covariances, as (Karnik & Tavoularis (1989))

$$-\overline{c^2 u_i} = D_{ij}\,\frac{\mathrm{d}c'^2}{\mathrm{d}x_j}. \tag{7}$$

These estimates, obtained as the best fits to pairs of maps of $\overline{c^2 u_i}$ and $\frac{\mathrm{d}c'^2}{\mathrm{d}x_j}$, have also been plotted in fig. 6. It can be seen that the two estimates of each diffusivity are generally close to each other, although it may be noted that the latter estimates have higher uncertainty than the former ones.

The evolution of D_{22} could be fitted by the power law $D_{22}/(U_C L) = 0.0013\,(x_1/L)^{0.6}$. At $x_1/L = 35$, $D_{22}/U_C L \approx 0.011 \pm 0.002$. The apparent diffusivity K_2 followed the same trend as D_{22}, but was generally about 25% larger. The other components of the turbulent diffusivity tensor appeared to approach the same growth rate as D_{22} far downstream of the source ($x_1/L > 25$; see figs. 6b-e). The asymptotic values of the ratios were

$$\frac{D_{ij}}{D_{22}} \approx \begin{bmatrix} -15 & -1.0 & 0 \\ 7.5 & 1.0 & 0 \\ 0 & 0 & 1.5 \end{bmatrix}. \tag{8}$$

$D_{33} \approx 1.5 D_{22}$, in conformity with the fact that $u_3' > u_2'$ and $\sigma_3 > \sigma_2$. The apparent diffusivity ratio was even higher ($K_3/K_2 = 2.0 \pm 0.3$). The variation of the turbulent Schmidt number $Sc_T \equiv \nu_T/D_{22}$ along the plume is presented in fig. 6f. This parameter approached the asymptote $Sc_T \approx 1.0 \pm 0.2$ for $x_1/L > 25$.

The strong anisotropy of the turbulence in USF is demonstrated by the fact that D_{11}, D_{22} and D_{33} have different values. Far downstream of the source, D_{11} was negative (*i.e.*, countergradient), levelling off to a magnitude that is an order of magnitude larger than D_{22}. Although $\left|d\overline{C}/dx_1\right| \ll \left|d\overline{C}/dx_2\right|$, the term $D_{11}\mathrm{d}\overline{C}/\mathrm{d}x_1$ was comparable in magnitude to $D_{12}\mathrm{d}\overline{C}/\mathrm{d}x_2$ in the core of the plume. D_{12} was nearly opposite to D_{22}, reflecting the fact that streamwise velocity fluctuations u_1, which contribute to the streamwise flux $\overline{cu_1}$, are strongly and negatively correlated to transverse fluctuations u_2 in USF. D_{21} appeared to be positive, albeit within considerable uncertainty as the term $D_{21}d\overline{C}/dx_1$ was considerably smaller than $D_{22}d\overline{C}/dx_2$.

Estimates of advection and diffusion

The molecular diffusion term in (eq. 1) was negligible, as the molecular diffusivity was several orders of magnitude smaller than the main turbulent diffusivities. In order to estimate the turbulent diffusion terms, smooth maps of $\overline{C}$, $\overline{cu_1}$, $\overline{cu_2}$, $\overline{cu_3}$ were created using eqs. 6 and 2 and the estimated turbulent diffusivities. The advection term $\overline{U_1}\partial\overline{C}/\partial x_1$ and the streamwise diffusive flux term $\partial\overline{cu_1}/\partial x_1$ were then determined applying first-order central differencing to data from five measurement planes. The in-plane diffusive flux terms, $\partial\overline{cu_2}/\partial x_2$ and $\partial\overline{cu_3}/\partial x_3$, were determined using second-order central difference methods.

Fig. 7 shows that the advection term was roughly equal to the net (total) diffusion term. Because these terms were determined from independent measurements, this observation attests to the overall accuracy of the present experimental results. The transverse and spanwise diffusive fluxes were nearly equal around the plume axis, but each became dominant off-axis, in regions in which the corresponding mean concentration derivative was dominant. The streamwise diffusive flux was consistently an order of magnitude smaller than the other two diffusive fluxes and made a very small contribution (less than 5%) to the net diffusion. This provides justification for disregarding streamwise diffusion, even though the corresponding diffusivity is much larger than the two other normal diffusivities.

Comparison to theoretical estimates

Analytical models of the turbulent diffusivity tensor relevant to USF have been developed by Tavoularis & Corrsin (1985), Rogers *et al.* (1989), and Younis *et al.* (2005), to be referred to as TC, RMR and YSC, respectively. The corresponding expressions are summarized in table 1, whereas ratios of the predicted diffusivity values are compared to the present results in table 2. All models assumed that $D_{31} = D_{13} = D_{32} = D_{23} = 0$ by symmetry of the Reynolds stress tensor about the $(x_1 - x_3)$ plane.

The TC model contains the Lagrangian integral timescales $\mathcal{T}_{11}$ *etc.*. We have no measurements of these timescales in the present flow, but we used the estimates $\mathcal{T}_{22} \approx 1.3 L_{22}/u_2'$ (Karnik & Tavoularis, 1990) and $\mathcal{T}_{12} = \mathcal{T}_{21} = 4\mathcal{T}_{22}$, $\mathcal{T}_{11} = 2\mathcal{T}_{22}$, and $\mathcal{T}_{33} = \mathcal{T}_{22}$ (TC), all applicable to USF. The RMR model is very similar to the TC model, however, the former contains a constant timescale $\mathcal{T} = \frac{1}{C_D}\frac{2k}{\varepsilon}$, in which $C_D = 12.6$ for the present conditions (C_D is specified by RMR as a function mainly of a Reynolds number and, weakly, of the Prandtl number). The YSC model is more complex than either of the two other models, expressing the diffusivities in terms of relationships that contain four adjustable coefficients, for which YSC recommend values.

All models predicted values of D_{22} which were more than double the measured value and ratios D_{33}/D_{22} that were close to the experimental ones. The TC prediction of D_{11}/D_{22} agreed in sign with the measured ratio although was smaller in magnitude, whereas the two other models missed this ratio not only in magnitude, but in sign as well. All models predicted D_{12}/D_{22} that had the same sign as the measured value but were roughly twice as large. The RMR and YSC models predicted a negative value of D_{21}/D_{22}, whereas the TC model predicted a value of zero; however, the measured D_{21}/D_{22} tended to be positive.

Overall, all models had comparable performances, with the notable exception that the TC model was the only one to predict correctly the sign of D_{11}. None

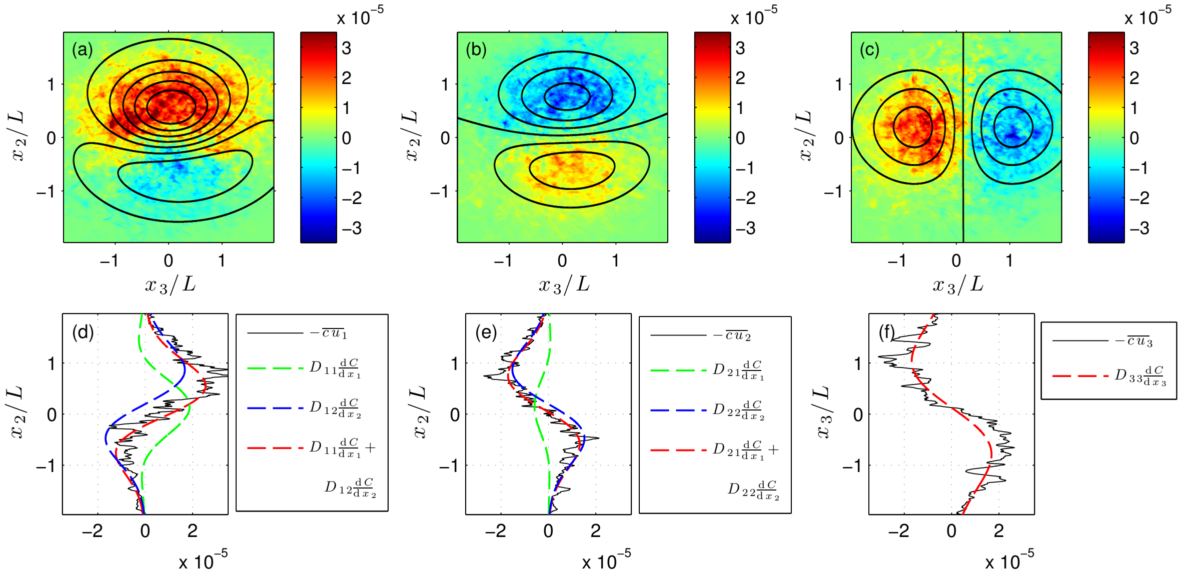

Figure 5: Maps of (a) $-\overline{cu_1}$, (b) $-\overline{cu_2}$, and (c) $-\overline{cu_3}$ at $x_1/L = 28$; black contour lines mark values fitted using eq. 2; (d-f) cross-sections of the maps compared to lines calculated from the fitted diffusivities; these figures also show corresponding individual terms of the right-hand side of eq. 2. All values are normalized by $C_S U_C$.

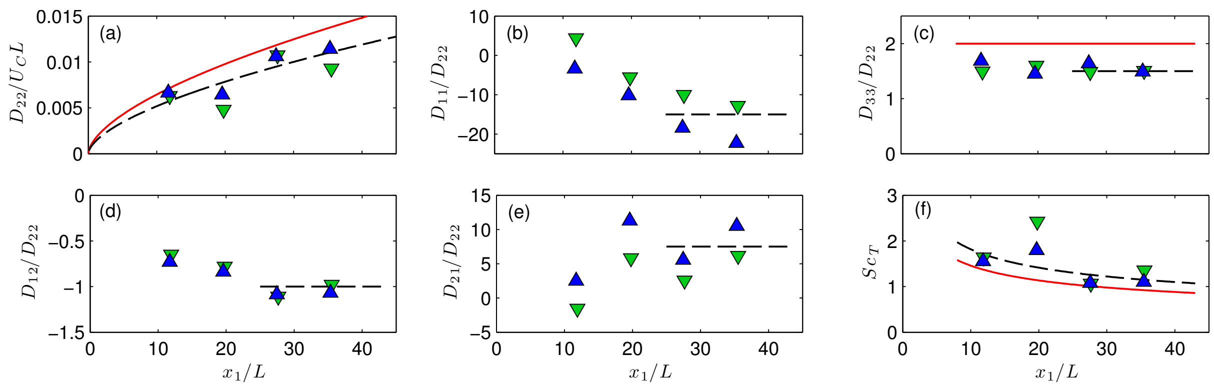

Figure 6: (a) The estimated diffusivity D_{22}, the fitted power law (dashed line), and the apparent diffusivity K_2 (—); (b-e) ratios of the turbulent diffusivities with dashed lines indicating their asymptotes, and the ratio K_3/K_2 (—); (f) estimates of the turbulent Schmidt number $Sc_T = \nu_T/D_{22}$, a smooth fit (dashed line), and the apparent Schmidt number ν_T/K_2 (—); ▲ and ▼ indicate diffusivities estimated from eq. 2 and eq. 7, respectively.

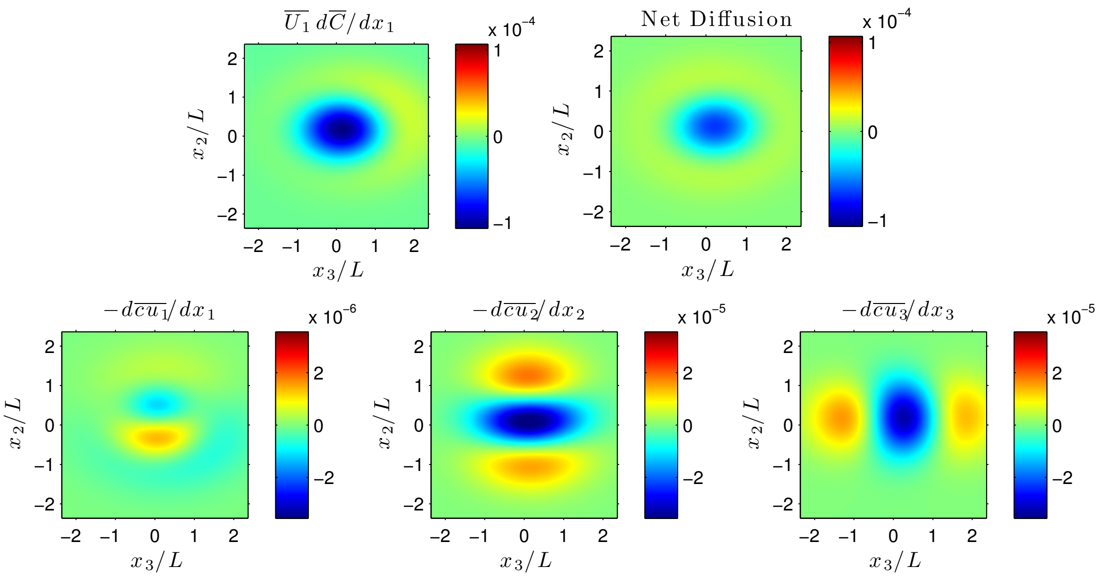

Figure 7: Maps of the advective and diffusive flux terms, normalized by $C_S U_C/L$ at $x_1/L = 28$.

Tavoularis & Corrsin (1985)	Rogers *et al.* (1989)	Younis *et al.* (2005)
$D_{11} = \overline{u_1^2}\,\mathcal{T}_{11} + \frac{dU_1}{dx_2}\,\overline{u_1u_2}\,\mathcal{T}_{12}^2$	$D_{11} = \overline{u_1^2}\,\mathcal{T} - \frac{dU_1}{dx_2}\,\overline{u_1u_2}\,\mathcal{T}^2$	$D_{11} = \overline{u_1^2}\left(C_2\frac{k}{\varepsilon}\right) + \frac{dU_1}{dx_2}\,\overline{u_1u_2}\left(2C_4\frac{k^2}{\varepsilon^2}\right) + C_1\frac{k^2}{\varepsilon}$
$D_{12} = \overline{u_1u_2}\,\mathcal{T}_{12}$	$D_{12} = \overline{u_1u_2}\,\mathcal{T} - \frac{dU_1}{dx_2}\,\overline{u_2^2}\,\mathcal{T}^2$	$D_{12} = \overline{u_1u_2}\left(C_2\frac{k}{\varepsilon}\right) + \frac{dU_1}{dx_2}\,\overline{u_2^2}\left(C_4\frac{k^2}{\varepsilon^2}\right) + C_3\frac{k^3}{\varepsilon^2}\frac{dU_1}{dx_2}\overline{u_2^2}$
$D_{21} = \overline{u_1u_2}\,\mathcal{T}_{21} + \frac{dU_1}{dx_2}\,\overline{u_2^2}\,\mathcal{T}_{22}^2$	$D_{21} = \overline{u_1u_2}\,\mathcal{T}$	$D_{21} = \overline{u_1u_2}\left(C_2\frac{k}{\varepsilon}\right) + \frac{dU_1}{dx_2}\,\overline{u_2^2}\left(C_4\frac{k^2}{\varepsilon^2}\right)$
$D_{22} = \overline{u_2^2}\,\mathcal{T}_{22}$	$D_{22} = \overline{u_2^2}\,\mathcal{T}$	$D_{22} = \overline{u_2^2}\left(C_2\frac{k}{\varepsilon}\right) + C_1\frac{k^2}{\varepsilon}$
$D_{33} = \overline{u_3^2}\,\mathcal{T}_{33}$	$D_{33} = \overline{u_3^2}\,\mathcal{T}$	$D_{33} = \overline{u_3^2}\left(C_2\frac{k}{\varepsilon}\right) + C_1\frac{k^2}{\varepsilon}$

Table 1: Theoretical models of the turbulent diffusivities.

	TC	RMR	YSC	present
D_{22}/D_{22m}	2.9	2.1	3.5	1.0
D_{11}/D_{22}	-10.0	2.8	3.4	-15.0
D_{33}/D_{22}	1.6	1.6	1.9	1.5
D_{12}/D_{22}	-2.0	-1.9	-1.8	-1.0
D_{21}/D_{22}	0.0	-0.5	-1.5	7.5

Table 2: Theoretical estimates of the turbulent diffusivity ratios; D_{22m} indicates the measured D_{22}.

of the models predicted accurately the magnitudes of the diffusivities, but predictions and measurements were of the same order of magnitude. It is noted that all models were developed and calibrated for air flows, in which the Prandtl/Schmidt numbers were of order one, whereas the present experiments were conducted at a very high Schmidt number.

CONCLUSIONS

Simultaneous concentration and velocity maps in the plume of a continuous point source in uniformly sheared turbulence have been constructed from measurements. A gradient transport model with a tensorial diffusivity described well the relationship between the measured turbulent mass flux vector and the mean concentration gradient. For the first time, all non-vanishing components of the turbulent diffusivity tensor were determined simultaneously from experimental results. The apparent diffusivities had the same trends as the corresponding normal diffusivities on a transverse plane, but the former were measurably larger. Ratios of the components of the turbulent diffusivity tensor tended to asymptotic values far downstream of the source. Three previous theoretical models of turbulent diffusion in shear flows had some qualitative agreement with the present results, especially the model of Tavoularis & Corrsin (1985), which predicted the negative value of D_{11}. The advection term in the advection-diffusion equation was roughly equal to the net diffusion term, attesting to the overall accuracy of the present experimental results.

REFERENCES

Arya, S.P. 1999 *Air Pollution Meteorology and Dispersion*. Oxford University Press, New York.

Batchelor, G.K. 1949 Diffusion in a field of homogeneous turbulence. I. Eulerian analysis. *Aust. J. Chem.* **2** (4), 437–450.

Corrsin, S. 1974 Limitations of gradient transport models in random walks and in turbulence. *Adv. Geophys.* p. 25.

Gendron, P.O., Avaltroni, F. & Wilkinson, K.J. 2008 Diffusion coefficients of several rhodamine derivatives as determined by pulsed field gradient–nuclear magnetic resonance and fluorescence correlation spectroscopy. *J. Fluoresc.* **18** (6), 1093–1101.

Karnik, U. & Tavoularis, S. 1989 Measurements of heat diffusion from a continuous line source in a uniformly sheared turbulent flow. *J. Fluid Mech.* **202**, 233–261.

Karnik, U. & Tavoularis, S. 1990 Lagrangian correlations and scales in uniformly sheared turbulence. *Phys. Fluids A* **2** (4), 587–591.

Nakamura, I., Sakai, Y., Miyata, M. & Tsunoda, H. 1986 Diffusion of matter from a continuous point source in uniform mean shear flows (1st report). *B. JSME* **29** (250), 1141–1148.

Riley, J.J. & Corrsin, S. 1974 The relation of turbulent diffusivities to Lagrangian velocity statistics for the simplest shear flow. *J. Geophys. Res.* **79** (12), 1768–1771.

Roberts, P.J.W. & Webster, D.R. 2002 Turbulent diffusion. In *Environmental Fluid Mechanics: Theories and Applications* (ed. H. Shen), pp. 7–45. American Society of Civil Engineers.

Rogers, M.M., Mansour, N.N. & Reynolds, W.C. 1989 An algebraic model for the turbulent flux of a passive scalar. *J. Fluid Mech.* **203** (1), 77–101.

Sreenivasan, K.R., Tavoularis, S. & Corrsin, S. 1982 A test of gradient transport and its generalizations. In *Turbulent Shear Flows 3* (ed. Bradbury, Durst, Launder, Schmidt & Whitelaw), pp. 96–112. Springer Berlin Heidelberg.

Tavoularis, S. & Corrsin, S. 1985 Effects of shear on the turbulent diffusivity tensor. *Int. J. Heat Mass Trans* **28** (1), 265–276.

Vanderwel, C. & Tavoularis, S. 2011 Coherent structures in uniformly sheared turbulent flow. *J. Fluid Mech.* **689**, 434–464.

Webster, D.R., Rahman, S. & Dasi, L.P. 2003 Laser-induced fluorescence measurements of a turbulent plume. *J. Eng. Mech.-ASCE* **129**, 1130–1137.

Younis, B.A., Speziale, C.G. & Clark, T.T. 2005 A rational model for the turbulent scalar fluxes. *Proc. R. Soc. A* **461**, 575–594.